A causal look into the quantum Talbot effect

A. S. Sanz* and S. Miret–Artés†
Instituto de Matemáticas y Física Fundamental
Consejo Superior de Investigaciones Científicas
Serrano 123, 28006 Madrid, Spain
(Dated: February 27, 2007)

The Talbot effect is a known phenomenon in both optics and quantum mechanics with a very simple physical explanation behind: near–field interference. This work is aimed to provide an insightful picture for this phenomenon in terms of Bohmian mechanics as well as for its classical limit, thus showing which are the causal reasons and conditions that lead to its appearance. To illustrate the theory, results obtained for diffraction of thermal He atoms by both an N–slit array and a weak corrugated Cu(110) surface are analyzed and discussed. Moreover, we show that the presence of short–range attractive interactions lead to a local increase of the so–called Talbot distance. We call this distortion caused by the short–range interaction (either attractive or repulsive) between the diffracted particles and the grating the Talbot–Beeby effect, which should be observable when looking at relatively close distances from the latter.

PACS numbers:

I. INTRODUCTION

Particle diffraction has become a standard technique to test the validity of quantum mechanics. This is confirmed by a large amount of experiments, ranging from tiny objects (e.g., electrons, neutrons, single atoms, or small clusters) to more complex, mesoscopic–size systems (e.g., fullerenes, large biomolecues, or Bose–Einstein condensates). In particular, it seems from the latter that there are no size–dependent obstacles to observe particle diffraction except those arising when trying to keep the coherence of their many degrees of freedom. This makes that large objects constitute an important benchmark to jump into the technological possibilities that diffraction has and can have in fields such as surface science, molecular physics, or quantum computation and quantum information, for instance.

In 1836, when characterizing optical gratings, Talbot[1] observed a repetition of alternate color bands of complementary colors (red and green, and blue and yellow) at certain distances from the grating. In 1881, about 50 years later, by means of optical arguments Rayleigh[2] found that this phenomenon was a consequence of the diffraction of a highly spatially coherent plane wave by the grating. After getting diffracted, the information carried by the outgoing wave about both the grating periodicity and the shape of each periodic unit that constitutes it results in such a nice color band structure. The alternation of color bands occurs at a periodic distance $z_T = d^2/\lambda$, known as the *Talbot distance*, where d and λ are the grating period and the wavelength of the incident beam, respectively; bands with the same color therefore repeat at integer multiples of twice the Talbot distance, $2z_T = 2d^2/\lambda$. This effect has important technological applications in optics, such as optical image processing, optical testing, or production of optical elements. In the same way, its quantum–mechanical counterpart is also relevant in electron optics, where it has many applications to electron microscopy. Nonetheless, it has also been observed experimentally with heavier particles than electrons, as shown by Chapman *et al.*[3] with Na atoms, or by Deng *et al.*[4] with Bose–Einstein condensates.

As in optics, an N–slit array can also be considered as a typical example of a grating in quantum mechanics. When this array is illuminated by a continuous, coherent beam, a continuous flow behind the slits is observed. The type of space structure formed is called a *carpet*[5] due to the distinctive periodic pattern that it displays. The periodicity of a carpet occurs at integer multiples of d along the direction parallel to the plane containing the slits (x), and $2z_T$ along the propagation direction (z). The repetitions found along z are called *recurrences*, and are separated a distance z_T. A recurrence that coincides with the initial state describing the (diffracted) system is called a *revival* of such a state, and appear at integer multiples of z_T; for even integers the state looks like exactly the same as the initial one, while for odd integers it is shifted half a period ($d/2$) with respect to the latter. Recurrences at fractions of z_T result in superposed images of the initial state with itself. Indeed, if the boundary conditions of the slits are "sharp" (the *window function* is not differentiable at the borders of the slit), one can observe *fractal* structures (i.e., structures such that enlargements of parts of them look like the whole one) at irrational fractions of z_T. In such cases, we have *fractal carpets*.[5,6,7,8,9]

A nice illustration of a Talbot carpet is displayed in Fig. 1(a). This carpet arises after diffracting a monochromatic beam of He atoms ($E_0 = 21$ meV) by a grating consisting of 50 Gaussian slits and a period $d = 3.6$ Å. The x axis is normalized to the grating period, d, and the z axis to twice the Talbot distance, $2z_T$ ($z_T = 13.08$ Å). The carpet appears when we record $\rho(x, z(t)) = |\Psi(x, z(t))|^2$ along x at different times, monitored in terms of z, since the wave propagates ahead at a constant speed (see below for details). That is, at each z we have kept the

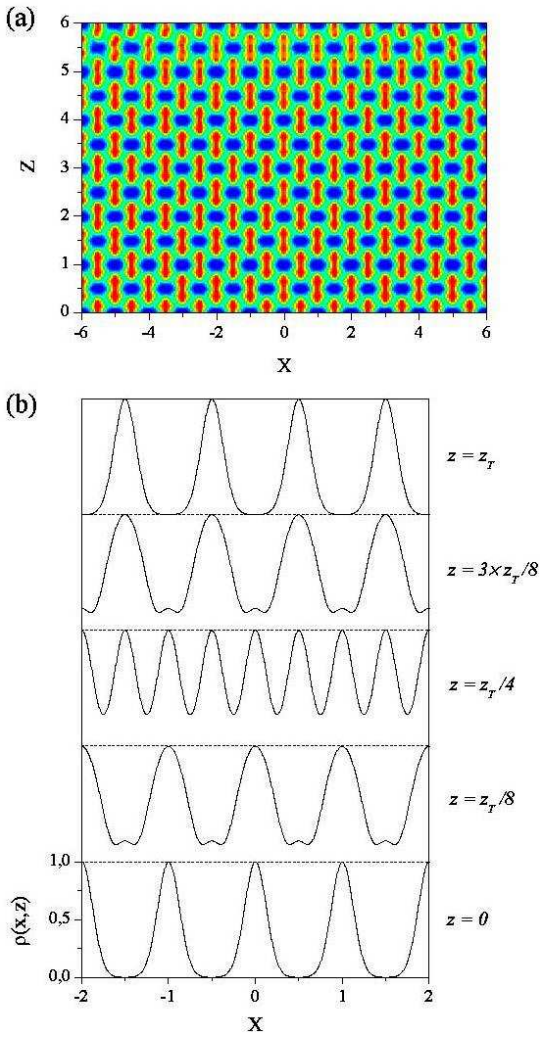

FIG. 1: (Color online.) (a) Quantum carpet for He diffracted by a 50–slit array. The color scale, from blue to red, indicates increasing values of the probability density. (b) Snapshots of the evolution of the probability density from $z = 0$ to $z = z_T$. In both panels, the x–distance is scaled in units of the grating period (d), and z in units of twice the Talbot distance ($2z_T = 2d^2/\lambda$).

"slice" $\rho(x, z(t))$ of the probability density. Some of these "slices" are shown in Fig. 1(b), from $z = 0$ to $z = z_T$. As seen, effectively, there is a revival of the initial state at z_T (shifted half a period), while the other "slices" only keep some vague reminiscence of $\rho(x, 0)$. After the diffracted beam reaches $z = z_T$, it will evolve towards $2z_T$ tracking the inverse sequence to the one shown in the figure [see Fig. 1(a)], and then giving rise to a true revival of the initial probability distribution. This process repeats endlessly unless the grating has finite periodicity, as happens with real gratings, whose limited extension causes the disappearance of the Talbot structure beyond a certain distance. In other words, since the Talbot effect is a typical near–field or Fresnel diffraction phenomenon, it will be significant provided the observation distance is of the order of (or less than) the grating size. Beyond such distance scales the carpet fades until it finally disappears, leading to the typical Fraunhofer patterns observed in most particle diffraction experiments.

Although Talbot patterns, such as that shown in Fig. 1(a), are well–known in the literature, as far as we know there is no a detailed explanation in causal terms. This work is aimed to provide a full causal interpretation for this phenomenon as well as for its relationship with the Fraunhofer diffraction and the classical limit. With this purpose we have chosen Bohmian mechanics, where the standard wave picture is replaced by trajectories in configuration space. The use of such trajectories is very important in order to render some light into real experiments, where a picture in terms of the motion of individual particles is always highly desirable (specially if these particles follow the quantum flow, unlike other classical representations). For example, this is an important issue in surface science experiments, where one is limited when illuminating a surface for its study and characterization. Note that surfaces can also be considered as gratings analogous to N–slit arrays because of their periodicity (when assuming that no imperfections are present). Nevertheless, the presence of a significant short–range interaction between the diffracted particles and the surface leads to a distortion of the period of the Talbot effect near the surface. We have called this effect the *Talbot–Beeby effect* because the variation of the wavelength associated to the diffracted beam under the presence of an attractive well is known in surface scattering as the *Beeby correction*.[10]

The organization of this work is as follows. In order to be self–contained, a rigorous and novel mathematical overview will be presented in Sec. II in terms of standard quantum mechanics, analyzing both the appearance of the Talbot effect for a Gaussian grating and the transition to the Fraunhofer regime. In Sec. III we will introduce the fundamentals of Bohmian mechanics and how this theory applies to the particular problem that we are dealing with here. A discussion of the Talbot and Talbot–Beeby effects in diffraction of He atoms by both an N–slit array and the Cu(110) surface is given in Secs. IV and V, respectively. In the light of these results, the meaning of the classical limit and the quantum–classical correspondence is discussed in Sec. VI. Finally, the main conclusions from this work are summarized in Sec. VII.

II. WAVE APPROACH TO THE TALBOT EFFECT

Rigorous analytical studies of the Talbot effect from an optical viewpoint can be found in the literature (see, for instance, Ref. 11). Here we provide an alternative quantum–mechanical derivation aimed to emphasize the physical aspects underlying this phenomenon, and that later will be used in the discussion of its Bohmian counterpart. In particular, two aspects are worth stressing:

(i) the role of the superposition principle, and (ii) the analogy/equivalence between Talbot structures and patterns observed in multimode cavities (e.g., waveguides).

For the sake of simplicity, we focus on gratings constituted by Gaussian slits,[12,13] i.e., those presenting a Gaussian transmission function. Nevertheless, our analysis can be generalized to any kind of periodic grating (of course, taking into account the geometry of such a grating). Gaussian transmissions can be observed, for instance, when considering an incident monochromatic beam (with wavelength λ) diffracted by a soft, repulsive (exponential) potential barrier with an infinity of identical holes (slits) of a certain width.[13] Assuming the initial time as the instant when the incident beam has just passed through the potential, the initial wave function can be represented as a coherent superposition of identical Gaussian functions, with centers at $x_0^{(k)} = kd$ ($k = 0$, ±1, ±2, ...) and $z_0^{(k)} = 0$, and propagating along the z direction, i.e., $p_x^{(k)} = 0$ and $p_z^{(k)} = 2\pi\hbar/\lambda$ (or, equivalently, $v_x^{(k)} = 0$ and $v_z^{(k)} = 2\pi\hbar/m\lambda$, respectively, where m is the mass of the incident particle). As will be shown below, such an initial wave function can be expressed as

$$\Psi(x,0) \propto \lim_{K\to\infty} A_x(0) \sum_{k=-K}^{K} e^{-(x-kd)^2/4\sigma_x^2}, \qquad (1)$$

where $A_x(0)$ is a constant given below and the Gaussian functions with the same width σ_x do not overlap (at $t = 0$). Moreover, unless otherwise stated, the total number of slits contributing in the sum can be expressed as $N = 2K + 1$, with a slit at $k = 0$.

We are also interested in the study of the He–Cu(110) scattering system, a simple case in surface science where the Cu(110) surface plays the role of the periodic grating. Therefore, we are going to assume that the grating period is the same as the periodicity of the Cu(110) surface, $d = 3.6$ Å, and He atoms will be the diffracted particles. Considering that the incidence energy of the He atom beam is $E_0 = E_z$ (normal incidence), we will have $p_z^{(n)} = \sqrt{2mE_z}$, with $\lambda = 2\pi\hbar/\sqrt{2mE_z}$. For example, if the incidence energy is $E_z = 21$ meV, the wavelength of the He beam will be $\lambda = 0.991$ Å, which is of the order of the grating period, this being a requirement to observe diffraction and interference phenomena.[12,13]

1. Single Gaussian slit

To understand the physics associated to the time–evolution of the diffracted wave function (1), first it is important to take into account some particular considerations concerning each single diffracted Gaussian function. Thus, let such a wave packet at $t = 0$ be

$$\Phi(x,z;0) = A(0)\, e^{-x^2/4\sigma_x^2 - z^2/4\sigma_z^2 + ip_z z/\hbar}, \qquad (2)$$

where $A(0) = (2\pi\sigma_x\sigma_z)^{-1/2}$ is the norm. The subsequent time–evolution of Φ is given by

$$\Phi(x,z;t) = A(t)\, e^{-x^2/4\tilde{\sigma}_{x,t}\sigma_x - (z-z_t)^2/4\tilde{\sigma}_{z,t}\sigma_z} \times e^{ip_z(z-z_t)/\hbar + iE_z t/\hbar}, \qquad (3)$$

where $A(t) = (2\pi\tilde{\sigma}_{x,t}\tilde{\sigma}_{z,t})^{-1/2}$, $z_t = v_z t$, $E_z = p_z^2/2m$, and

$$\tilde{\sigma}_{i,t} = \sigma_i \left(1 + \frac{i\hbar t}{2m\sigma_i^2}\right), \qquad i = x, z. \qquad (4)$$

According to the last expression, the instantaneous Gaussian width (in either direction) reads as

$$\sigma_{i,t} = |\tilde{\sigma}_{i,t}| = \sigma_i \sqrt{1 + \frac{\hbar^2 t^2}{4m^2\sigma_i^4}}, \qquad i = x, z. \qquad (5)$$

Thus, we can define a timescale $t_s = 2m\sigma_i^2/\hbar$ that separates two regimes with different "spreading rates". If $t \ll t_s$, the Gaussian width almost remains the same ($\sigma_{i,t} \approx \sigma_i$). On the other hand, if $t \gg t_s$, the Gaussian width undergoes a linear increase with time ($\sigma_{i,t} \approx \hbar t/2m\sigma_i$). In this way, choosing $\sigma_x = d/8$ and $\sigma_z = d$, the Gaussian functions will almost not display any increase in their size along z, but only along x, this allowing their overlapping (along this direction) and therefore the appearance of interference. With this, we express Eq. (3) as

$$\Phi(x,z;t) = A'(t)\, e^{-x^2/4\tilde{\sigma}_{x,t}\sigma_x - (z-z_t)^2/4\sigma_z^2} \times e^{ip_z(z-z_t)/\hbar + iE_z t/\hbar}, \qquad (6)$$

where $A'(t) = (2\pi\tilde{\sigma}_{x,t}\sigma_z)^{-1/2}$.

To further simplify, we assume $V(x,z) = 0$ everywhere except along the barrier ($z = 0$), where it is infinity. Thus, there is no coupling between both coordinates, x and z, and the time–evolution of the Gaussian function associated to each direction can be studied separately. Since the interference will take place along the x direction, we then only care about the part of the wave function depending on x,

$$\Phi_x(x,t) = A_x(t)\, e^{-x^2/4\tilde{\sigma}_{x,t}\sigma_x}, \qquad (7)$$

where $A_x(t) = (2\pi\tilde{\sigma}_{x,t}^2)^{-1/4}$. Regarding Φ_z, it is only important the fact that it propagates along z at a constant speed v_z. That is, at a time t the centroid of the Gaussian function (3) will be at $z = v_z t$. Because of this simplification, from now on we will omit the subscript x when referring to the wave function (Ψ or Φ instead of Ψ_x or Φ_x, respectively), the spreading along the x–direction [σ and A instead of σ_x and A_x, respectively], and the momentum associated to the x coordinate (p instead of p_x).

2. Infinite periodic slit gratings

According to Bloch's theorem,[14] the problem of finding the wave function associated to a given infinite periodic

potential reduces to determine the wave function associated to a single *unit cell* of such a potential; the full wave function is just a repetition of the latter, since it will satisfy the Born–von Karman boundary conditions,

$$\Psi(x+d,t) = \Psi(x,t). \tag{8}$$

It is clear that Eq. (1) is periodic with period d, and therefore we can obtain the interference properties directly from it by taking advantage of Bloch's theorem (i.e., without the need of going beyond a single unit cell).

Thus, let us consider the Gaussian wave packet with $k = 0$ and confined within the unit cell with $x = \pm d/2$, i.e., Eq. (7). We know that any unbound wave function can be represented as a superposition of plane waves,

$$\Psi(x,t) = \frac{1}{\sqrt{2\pi\hbar}} \int a(p)\, e^{ipx/\hbar - i\omega t}\, dp, \tag{9}$$

with

$$a(p) = \frac{1}{\sqrt{2\pi\hbar}} \int \Psi(x,0)\, e^{-ipx/\hbar}\, dx. \tag{10}$$

Thus, Eq. (7) can be expressed as

$$\Psi(x,t) = \frac{(8\pi\sigma^2)^{1/4}}{2\pi\hbar} \int e^{-\sigma^2 p^2/\hbar^2 + ipx/\hbar - i\omega t}\, dp. \tag{11}$$

However, because of the periodic boundary condition (8), not all momenta are allowed; we pass from a continuous basis of momenta to a discrete one, and (11) becomes

$$\Phi(x,t) = \sqrt{\frac{1}{d}} \left(\frac{8\pi\sigma^2}{d^2}\right)^{1/4} \sum_{|n|=1}^{\infty} e^{-\sigma^2 p_n^2/\hbar^2 + ip_n x/\hbar - i\omega_n t}, \tag{12}$$

where $p_n = 2\pi\hbar n/d$ and $\omega_n = 2\pi^2\hbar n^2/md^2$. As we will see below, this quantization condition to a unit cell carries important physical consequences (and differences with respect to a multimode cavity). Note that considering the time–dependence of Eq. (1), substituting (12) into the resulting expression, and rearranging terms leads to

$$\Psi(x,t) \propto \lim_{K\to\infty} (2K+1)\, \Phi(x,t). \tag{13}$$

That is, as one would expect, all the information regarding the infinite grating is contained within a single unit cell [as expressed by relation (8)]. The factor $2K+1$ (with $K \to \infty$) arises from the number of unit cells considered. Therefore, in order to keep the norm bound to unity, we should have

$$\Psi(x,0) = \lim_{K\to\infty} \frac{A(0)}{2K+1} \sum_{k=-K}^{K} e^{-(x-kd)^2/4\sigma^2}, \tag{14}$$

or, taking into account the time–dependence,

$$\Psi(x,t) = \lim_{K\to\infty} \frac{A_x(t)}{2K+1} \sum_{k=-K}^{K} e^{-(x-kd)^2/4\tilde{\sigma}_{x,t}\sigma}. \tag{15}$$

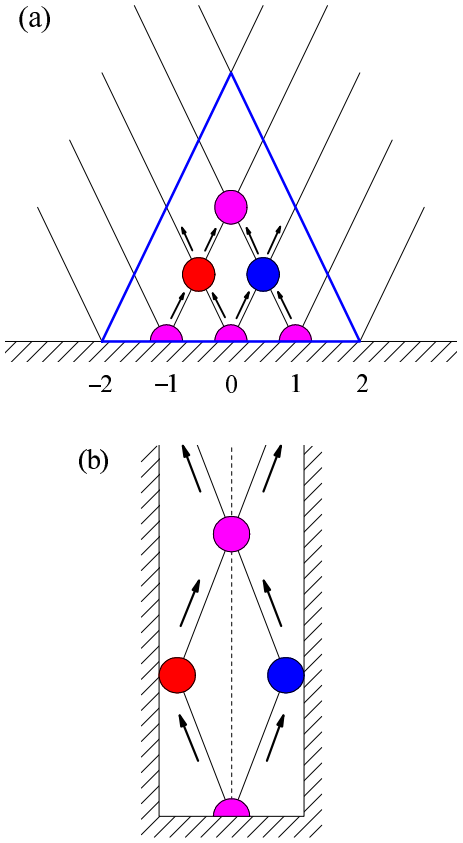

FIG. 2: (Color online.) Schematic picture of the appearance of revivals in: (a) a grating of Gaussian slits and (b) a multimode cavity. The arrows indicate the direction of the motion of the "interfering" disks (see text for details) and the straight lines represent the corresponding paths. In part (a), the numbers label the different slits, and the blue line encloses the Talbot area.

The smallest time elapsed necessary to observe a recurrence of the wave function is determined by the condition

$$\Psi(x, t+\tau_r) = \Psi(x,t). \tag{16}$$

From (12) it is straightforward to see that this condition is satisfied whenever $e^{-i\omega_n\tau_r} = e^{-2\pi i}$ for all n, i.e., when $\tau_r = 2\pi/\omega_1 = md^2/\pi\hbar$. At this time, the z–distance between two consecutive recurrences of $\Phi(x,t)$ will be $z_r = v_z\tau_r = 2d^2/\lambda$, i.e., twice the Talbot distance ($2z_T$). Note that this distance is the same that can be observed in Fig. 1(a) separating two recurrent slices of $\rho(x,t) = |\Psi(x,t)|^2$. However, as shown in Fig. 1(b), there are also recurrences with the periodicity of the Talbot distance. These recurrences result from considering the symmetry

$$\Psi(x + d/2, t + \tau_r/2) = \Psi(x,t), \tag{17}$$

which appears when taking the terms $e^{ip_n x/\hbar - i\omega_n\tau_r}$ as a whole. In this case, effectively, we observe that recurrences occur at the Talbot distance, $z_r = d^2/\lambda = z_T$.

The process that leads to observe revivals (and therefore recurrences) can be explained by means of the simple

schematic picture displayed in Fig. 2(a). To understand this picture, consider that each wave packet can be represented by two "interfering" hard disks that propagate ahead in z with opposite velocities in x (thus, the resulting x–motion of its center of mass is null, as expected from the true wave packet, which only advances along z). Note that these disks just indicate the spreading of the true wave packet width in both directions ($kd \pm x$). Tracking the motion of the disks departing from $k = 0$, we observe that they first meet at $\pm d/2$ and $z = z_T$ with those arriving from the neighboring slits ($k = \pm 1$). This causes the first revival, since all disks are identical and there will be full constructive "interference". As is apparent, the next revival will occur at $z = 2z_T$, and is caused by the disks coming from $k = \pm 1$, but not from $k = 0$ (which will contribute to the revivals observed at points $x = \pm d$ and $z = 2z_T$).

From Fig. 2(a) we can also infer an effective size for Talbot structures when the grating periodicity is limited. In the picture we have considered 5 slits, thus after the ingoing–moving disks corresponding to $k = \pm 5$ have interfered, no Talbot revivals will be observed anymore. From the point of view of the Gaussian wave packets, this will happen after the size of those corresponding to the outermost slits is large enough as to make them to interfere, i.e., when $2\sigma_t \approx 2Kd$. Assuming that at that stage the width of the Gaussian functions increases linearly with time, i.e., $\sigma_t \approx \hbar t/2m\sigma$, the maximum time to observe a revival will be $t_{\max} \approx 2Kdm\sigma/\hbar$. And, since the propagation along z is also linear with time, at the speed v_z, the maximum z–distance where the Talbot structure is still observable is

$$z_{\max} \approx v_z t_{\max} \approx 2z_T \, \frac{\pi(N-1)}{8} \tag{18}$$

(we have particularized this expression to our case, where $\sigma = d/8$). Examples of the validity of this relation will be seen in Sec. IV. Beyond $z_{\max}$ one starts to observe a transition towards the Fraunhofer diffraction regime, with its characteristic fringe patterns. Indeed, as seen in Fig. 2(a), this transition takes place beyond the boundaries marked by the triangle with height $z_{\max}$ and basis $(N-1)d$ (denoted with a blue line in the figure).

It is clear that as soon as the wave function (or part of it) leaves the Talbot region, neither Bloch's theorem nor the Born–von Karman boundary conditions are applicable anymore. Thus, in order to describe the Fraunhofer diffraction, one can start from Eq. (15), but neglecting the limit for K (N), since now the grating is assumed to have a finite size (remember that the Talbot effect arises precisely when considering an infinite periodic grating). At a relatively long z–distance from the grating, its dimensions are negligible when compared with the distances x involved in the diffraction process. That is, $x \gg (N-1)d$, and therefore

$$e^{-(x-kd)^2/4\tilde{\sigma}_t\sigma} \approx e^{-\sigma^2\kappa^2x^2/z^2} \, e^{i\kappa x^2/2z} \, e^{-ik\kappa dx/z}, \tag{19}$$

where $\kappa = 2\pi/\lambda$. Substituting the r.h.s. of this expression into Eq. (15) we reach

$$\Psi(x,t) \approx \frac{A(t)}{2K+1} \, e^{-\sigma^2\kappa^2x^2/z^2} \, e^{i\kappa x^2/2z} \sum_{k=-K}^{K} e^{-ik\kappa dx/z}. \tag{20}$$

Now, using the mathematical property

$$\sum_{s=1}^{S} e^{s\eta} = \frac{1-e^{S\eta}}{1-e^{\eta}}, \tag{21}$$

Eq. (20) becomes

$$\Psi(x,t) \approx A(t) \, e^{-\sigma^2\kappa^2x^2/z^2} \, e^{i\kappa x^2/2z} \, \frac{\sin\left(N\kappa d \sin\theta/2\right)}{N \sin\left(\kappa d \sin\theta/2\right)}, \tag{22}$$

where we have made use of the so–called paraxial approximation from optics,[15] and consider $x/z = \tan\theta \approx \sin\theta$, θ being the observation angle. Equation (22) is more conveniently expressed in terms of the probability density,

$$\rho(x,t) = |A(t)|^2 \, e^{-\sigma_x^2\kappa^2x^2/z^2} \left[\frac{\sin\left(N\kappa d \sin\theta/2\right)}{N \sin\left(\kappa d \sin\theta/2\right)}\right]^2, \tag{23}$$

as its optical counterpart, namely the diffracted intensity. In Eq. (23), the term between square brackets is the *structure factor*, which accounts for the interference effects and depends on the grating period and the number of unit cells. On the other hand, the remaining terms (the normalized exponential) is the *form factor*, which is related to the diffraction by a single unit cell. Because of the information provided by these factors, they are very useful to characterize optical grids[15] as well periodic surfaces.[14]

From the structure factor we observe that the Fraunhofer fringes appear in accordance to the diffraction (quantization) condition

$$\sin\theta = \ell \, \frac{\lambda}{d}, \qquad \ell = 0, \pm 1, \pm 2, \ldots \tag{24}$$

where ℓ is called the *diffraction order*. On the other hand, there will be a series of minima whenever

$$\sin\theta = \frac{\ell'}{N} \, \frac{\lambda}{d}, \qquad |\ell' - \ell| = 1, 2, \ldots, N-1. \tag{25}$$

Hence, there will be $N-1$ minima between two consecutive principal maxima and, consequently, $N-2$ secondary maxima (the height of these maxima is smaller than that of principal maxima and decreases very fast as N increases[12]).

Finally, a comment regarding the local spreading of each Gaussian wave packet and the boundary condition (8) is worth stressing. According to Eq. (7), after sometime the size of every Gaussian in (14) will be such that it will extend beyond the boundaries of its corresponding unit cell (indeed, as seen above, this leads to the appearance of the Fraunhofer diffraction when the grating periodicity is limited). That is, the spreading of the

Gaussian function, which is a local effect, gives rise to the appearance of a nonlocal behavior, where each part of the resulting wave function is strongly influenced by the presence of the remaining ones. Note, indeed, that the Talbot effect is precisely a nonlocal effect, since it emerges as a consequence of the overlapping or superposition of many identical wave packets. Nonetheless, one can still speak of a certain locality when considering Born–von Karman boundary conditions, and therefore the quantization of the whole wave function (14) into identical entities of the size of a unit cell. As will be seen below, Bohmian mechanics provides a natural picture to this problem in terms of two well–defined regimes of motion associated to a sort of dynamic equilibria.

3. *Multimode cavities*

The Talbot effect is very strongly related to the multimode interference[16,17] (for several fermions see Ref. 18), i.e., the interference process that takes place when an infinity of modes of a cavity are superposed. A typical multimode cavity is a waveguide, where the waves can be constrained in the x direction and unbound along the z direction. Assuming again no coupling between both degrees of freedom, the evolution of such a system can be described by Eq. (7). Thus, if the waveguide along the x direction is a square box centered at $x = 0$ and with length d, the boundary condition for the wave function will be that it has to vanish at $x = \pm d/2$. This wave function can be expressed at any time as

$$\Phi(x,t) = \sqrt{\frac{8}{d}}\left(\frac{2\pi\sigma^2}{d^2}\right)^{1/4} \times \sum_{n=0}^{\infty} e^{-\sigma^2 p_n^2/\hbar^2 - iE_n t/\hbar}\cos(p_n x/\hbar), \quad n = 0,1,2,\ldots \tag{26}$$

with $p_n = (2n+1)\pi\hbar/d$ and $E_n = p_n^2/2m$. It is easy to show[19] that recurrences in the probability density arising from (26) occur at integer multiples of the period associated to the smallest frequency. In our case, this frequency is $\omega_{1,0} = 4\pi^2\hbar^2/md^2$, and the period associated is

$$\tau_r = \frac{2\pi}{\omega_{1,0}} = \frac{md^2}{2\pi\hbar}. \tag{27}$$

We have to mention that the same periodicity can also be observed in the wave function, expect for a constant phase factor [$\Phi(x, t+\tau_r) = e^{i\varphi}\Phi(x,t)$].

Since the wave function evolves at a constat speed along z (i.e., along the channel of the waveguide), the recurrences will also give rise to the formation of quantum carpets; some examples of these carpets can be found, for instance, in Ref. 12. These recurrences appear at integer multiples of the distance $z_r = v_z\tau_r = d^2/\lambda$, which corresponds to the Talbot distance obtained in the case of a periodic grating. It is important to stress that here revivals only occur with this periodicity. In other words, this is the analogous case to the revivals observed at $z = 2z_T$ in a grating. Nevertheless, the probability density can still display another recurrence at $\tau_r/2$ because the wave function satisfies the following symmetry:

$$\Phi(x, t+\tau_r/2) = -e^{i\varphi}\Phi(x,t) \implies \rho(x, t+\tau_r/2) = \rho(x,t) \tag{28}$$

(which is also present in a periodic grating, although it is not relevant because it does not lead to the observation of revivals, as happens here).

Understanding why one cannot observe the same type of recurrences in a waveguide at z_T and $2z_T$ than in periodic grating is very apparent by looking at Fig. 2(b). This picture is equivalent to that shown in Fig. 2(a), but showing that the only possibility for the disks to cross is when they meet again, since no interference at $x = \pm d/2$ is possible. Note that, if we consider the disks as distinguishable, when they interfere at $z = z_T$, they are moving in opposite directions with respect to their initial motion (at $z = 0$). Thus, in order to recover the same state of motion, one has to wait until $z = 2z_T$. Nonetheless, this is only a sort of illusion based on a classical picture. As the Bohmian picture will show, in quantum mechanics such a possibility is discarded. In any case, it is important to stress that here the frequency quantization does not arise from having periodicity, but impenetrable walls.

III. BOHMIAN APPROACH TO THE TALBOT EFFECT

The fundamental equations of Bohmian mechanics are commonly derived by writing the system wave function in polar form,[20,21,22]

$$\Psi(x,t) = \rho_t^{1/2}\,\mathrm{e}^{\mathrm{i}S_t/\hbar}, \tag{29}$$

with $\rho_t = \rho(x,t)$ being the probability density and $S_t = S(x,t)$ the (real–valued) phase, and substituting it into the Schrödinger equation. This leads to two (real–valued) couple differential equations

$$\frac{\partial\rho_t}{\partial t} + \nabla\cdot\left(\rho_t\,\frac{\nabla S_t}{m}\right) = 0, \tag{30}$$

$$\frac{\partial S_t}{\partial t} + \frac{(\nabla S_t)^2}{2m} + V + Q_t = 0. \tag{31}$$

Equation (30) is a continuity equation that ensures the conservation of the flux of quantum particles. Nevertheless, more interesting from a dynamical viewpoint is Eq. (31), which is a quantum Hamilton–Jacobi equation governing the motion of particles under the action of a total effective potential $V_t^{\mathrm{eff}} = V + Q_t$. The last term in the l.h.s. of this equation is the so–called *quantum potential*,

$$Q_t = -\frac{\hbar^2}{2m}\frac{\nabla^2\rho_t^{1/2}}{\rho_t^{1/2}}. \tag{32}$$

This context–dependent, non–local potential determines together with V the total force acting on the system.

In the classical Hamilton–Jacobi theory, S_t represents the action of the system at a time t, and the trajectories describing the evolution of the system correspond to the paths perpendicular to the constant–action surfaces at each time. Analogously, since the Schrödinger equation can be rewritten in terms of the Hamilton–Jacobi equation (31), S_t can be interpreted as a quantum action satisfying similar mathematical requirements as its classical homologous. The classical concept of trajectory emerges then in Bohmian mechanics in a natural way, defining the particle trajectory as

$$\dot{x} = \frac{\nabla S_t}{m} = \frac{\hbar}{m}\ \mathrm{Im}\left[\Psi^{-1}\nabla\Psi\right] \tag{33}$$

(the same holds for the z–coordinate). Since in Bohmian mechanics the system consists of a wave and a particle, it is not necessary to specify the initial momentum for the particles, as happens in classical mechanics, but only their initial position, x_0, and the initial configuration of the wave function, $\Psi(x,0)$. The initial momentum field is predetermined by $\Psi(x,0)$ via Eq. (33), and the statistical predictions of the standard quantum mechanics are reproduced by considering an ensemble of (non–interacting[23]) particles distributed according to the initial probability density, $\rho(x,0)$.

Equation (33) is well defined provided that the wave function is continuous and differentiable. This is not the case, however, for quantum fractals,[6,7,8,9] where the Bohmian mechanics based on (33) is unable to offer a trajectory picture for such type of wave functions. This apparent incompleteness can be nevertheless "bridged" by taking into account the decomposition of the quantum fractal as a sum of (differentiable) eigenvectors of the corresponding Hamiltonian, and then redefining equation (33) in a convenient way. This can be seen in detail in Ref. 19, where a generalization of the standard formulation of Bohmian mechanics to include quantum fractals is given, and hence it will not be reviewed here since it would go beyond the scope of this work.

Except in a few very simple systems[21] (e.g., plane waves, free Gaussian wave packets, the harmonic oscillator, or stationary states), obtaining an analytical solution to Eq. (33) is impossible for most of the problems of interest due to their high nonlinearity. This is the case, for example, of multiple slit systems, where the wave analysis is rather simple, but its Bohmian counterpart needs of computational help. Nevertheless, getting some physical insight is still possible by studying the properties of the velocity field. Indeed, the fact that Bloch's theorem (together with the Born–von Karman boundary conditions) holds simplifies this study from both a conceptual and a computational sense. Conceptually, because the study of the full system reduces to only understand the dynamics within a single unit cell. In this sense, the analysis is similar to that of having a multimode cavity, as said above. On the other hand, this also brings a computational counterpart, since it also allows to perform calculations taking into account a single unit cell and periodic boundary conditions [i.e., $\Psi(x-d/2)=\Psi(x+d/2)$], thus reducing the time of computation. Of course, this simplification is only possible if we are under the assumption of infinite periodic gratings or, at least, we are working within the Talbot area, delimited by the triangle shown in Fig. 2(a). Otherwise, such an advantageous framework is no longer valid, and one has to consider the full system.

According to the previous prescription, after substituting Eq. (12) into (33), we obtain

$$\dot{x} = \frac{1}{m}\frac{\sum_{i,j} p_i\, e^{-\sigma^2(p_i^2+p_j^2)/\hbar}\cos[(p_i-p_j)x/\hbar-(\omega_i-\omega_j)t]}{\sum_{i,j} e^{-\sigma^2(p_i^2+p_j^2)/\hbar}\cos[(p_i-p_j)x/\hbar-(\omega_i-\omega_j)t]}, \qquad i,j=\pm1,\pm2,\ldots \tag{34}$$

It is not necessary to integrate this equation in order to get some relevant information about the physical properties of the quantum trajectories (i.e., their topology). Thus, first note that the velocity field (34) satisfies exactly the same symmetry conditions given by the relations (16) and (17). Taking this into account, one infers that the particle motion will be oscillatory, with the recurrences being the space regions where particles accumulate and therefore produce maxima in $\rho(x,t)$. However, also note that unlike the disks depicted in Fig. 2(a), the trajectories belonging to a single unit cell will remain within this unit cell. In other words, trajectories from different unit cells never mix.

The previous property is a manifestation of the *non–crossing property* of Bohmian mechanics: trajectories can never pass through the same space point at the same time due to the single–valuedness of the momentum field. From a Bohmian viewpoint this means that somehow the unit cell behaves as a multimode cavity, with the boundary periodic conditions giving rise to the presence of a nonphysical *impenetrable* walls at $x=\pm d/2$. Observe that at these points ($x=\pm d/2$), the velocity field (34) vanishes and therefore the corresponding quantum trajectories will be just straight lines, which due to the non–crossing property will act as (impenetrable) boundaries for particles coming from different neighboring unit

cells. This can be regarded as the Bohmian interpretation of the Born–von Karman periodic boundary conditions. Nonetheless, note that this effect also happens for the trajectory started at $x = 0$ (again the velocity field is zero). Accordingly, we find another (impenetrable) barrier that separate two specular (with respect to $x = 0$) regimes of motion. This goes even beyond the picture provided by the disks in Fig. 2(b) for the multimode cavity, since it adds another constraint to the types of motion that one can observe in quantum mechanics (or, equivalently, to the topology of the trajectories). Note that this behavioral pattern is regardless the motion along the z direction, where all Bohmian particles present the same uniform rectilinear motion,

$$z(t) = z_0 + v_z t, \tag{35}$$

as in classical mechanics. This is because the dynamics of the swarm of particles is basically directed by a plane wave (the Gaussian profile does not vary too much according to the assumption given above).

If a size–limited grating is considered, after some time the trajectories will be out of the Talbot area, and therefore the description given above will no longer be applicable. Dealing with Eq. (34) along the transition regime is an intractable problem. However, far beyond the grating, one can appeal to the Fraunhofer approximation in order to get again some insight on the topology presented by the trajectories. In such a case, introducing Eq. (22) into (33) leads to

$$\dot{x} \approx \frac{\hbar\kappa}{m}\frac{x}{z} = v_z\,\frac{x}{z}. \tag{36}$$

Assuming that the probability density is only significant along the quantized values of $x/z \approx \sin\theta$, where one observes the Fraunhofer principal maxima (we neglect the presence of secondary maxima), Eq. (36) can be rewritten as

$$\dot{x} \approx \ell v_z\,\frac{\lambda}{d}. \tag{37}$$

This assumption is equivalent to consider that the diffracted wave function consists of different independent plane waves, each one characterized by a momentum $p_\ell = \ell(2\pi\hbar/d)$, i.e., the Talbot quantized momenta. This is a very important result that can be understood in terms of two different equilibrium regimes. The first equilibrium regime occurs in the Talbot/Fresnel region, and is characterized by what we could call an *equilibrium of momenta*. That is, in this region the possible momenta satisfying a certain quantization condition are selected. This selection depends on the features defining the unit cell of the grating. For example, in atom–surface scattering systems one takes advantage of this fact to extract information about the diffraction process once the classical interaction potential, V, has vanished (what happens at a few Ångstroms from the surface).

On the other hand, there is a second equilibrium regime which we could call *equilibrium of configuration*. It happens far beyond the grating, once the particle distribution remains with the same shape (regardless spreading effects). The transition from the momentum equilibrium to the configuration one is a direct consequence of the rearrangement of moment among the different particles contributing to $\rho(x,t)$. These momenta make $\rho(x,t)$ to evolve in such a manner that at a certain distance from the grating, they will split the wave function into different wave packets, each moving with a different momentum $p_\ell = \ell(2\pi\hbar/d)$. That is, the equation of motion for the particles will be

$$x(t) \approx x_0 + \frac{2\pi\hbar\ell}{md}\,t, \tag{38}$$

where $\ell = 0$ denotes the classical direction of motion, i.e., without deviation. Note that as m increases, this deviation gets smaller, as corresponds to a classical particle.

As we have seen, the non–crossing property leads one to think of the effects caused by systems such as periodic gratings in terms of some effective impenetrable barriers when appealing to Bohmian mechanics. Nonetheless, on the other hand, one can also consider that the effect of higher increase in the number of trajectories in a certain region is conditioned by an *effective quantum pressure*: the trajectories moving along the impenetrable barrier will keep their motion until those arriving from the central part of the initial wave packet will move towards $x = 0$, thus decreasing the "pressure" exerted on the former (the same effect has been discussed in multimode cavities[19] or soft double slits[13]). Moreover, for finite gratings, this pressure is also the responsible for the appearance of the Fraunhofer fringes; after all wave packets have interfered means, in Bohmian terms, a decrease of the quantum pressure. Thus, the trajectories start to abandon their motion within the Talbot structure, and emerge into different channels until they reach a sort of equilibrium state, in which they move along different channels. These are the well–known (Fraunhofer) diffraction channels.

Non–crossing, effective infinite barriers, or quantum pressure, all of these are intertwined effects related to the topology of the quantum trajectories. Below we will illustrate them by analyzing the diffraction of He atoms by gratings constituted by N–slit systems and also the periodic, weakly corrugated Cu(110) surface.

IV. SLIT ARRAYS

First we consider the dynamics provoked by slit arrays, where He atoms are the diffracted particles and the slits are described by Gaussian (transmission) functions.[12,13] In Fig. 3(a) we can observe that, in accordance to the previous discussion in Sec. III, the trajectories follow the flow characterizing ρ_t in Fig. 1(a). Note that here the *trajectory carpet* is not a one–piece structure, as happened with the Talbot carpet generated by ρ_t in Fig. 1(a), but it consists of many unit substructures, as many as slits have

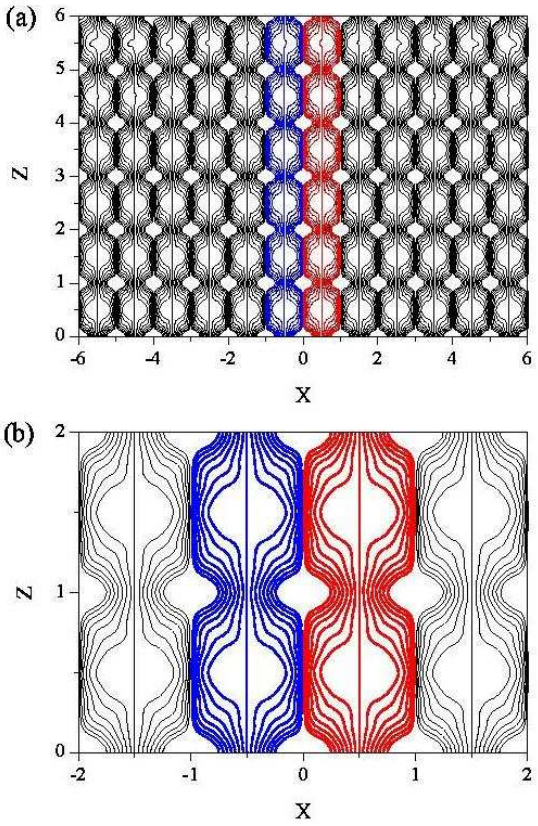

FIG. 3: (Color online.) (a) Quantum trajectories associated to Fig. 1(a). Trajectories in different color indicate that though according to Fig. 1(a) the Talbot carpet seems to be a one–piece pattern, it is indeed constituted by many single bunches of trajectories arising from each slit and without crossing with those exiting from neighboring slits. (b) Enlargement of Fig. 3(a) in the region close to the slits in order to show the correspondence with Fig. 1(b). In both panels, the x–distance is scaled in units of the grating period (d), and z in units of twice the Talbot distance ($2z_T$).

been considered. Moreover, trajectories exiting from one of the slits never cross those leaving the other slits, this being due to the non–crossing property described above. This can be better seen by looking at the enlargement presented in Fig. 3(b). In this plot we observe that initially the trajectories leave the slit in a diffusive manner towards each border of the slit. Since all the slits are identical (as well as their transmission function), the trajectories will feel in a short term the presence of bunches of trajectories coming from the neighboring slits. Then, the trajectories start bending until they move perpendicularly to the slits for a while, pushed by the neighboring trajectories. This is a clear manifestation of the quantum pressure: the pressure exerted by bunches of trajectories moving in opposite directions gives rise to an effect similar to that of having an impenetrable (infinite) potential barrier. But the quantum pressure is also felt from the action of the trajectories coming from the same slit: those started with initial conditions closer to the center of the slit with push the other to move parallel; only when they start moving back again towards the central axis of the slit, the quantum pressure will decrease enough as to allow the outer trajectories to move again towards the original position of the slit. In this way, at $z = 2z_T$ we will recover again the initial pattern of a sum of Gaussians. It is interesting to stress that the maxima at $z = z_T$, shown in Fig. 1(b), have not the same constitution as those at $z = 0$ or $z = 2z_T$: in this case, the trajectories contributing to the maxima belong to two different (neighboring) unit cells, while in the latter cases the trajectories belong to the same unit cell.

Provided the grating extends to infinity, the extension of the unit structures of the pattern seen in Fig. 3(a) repeat indefinitely. However, it is obvious that standard slits have a limited size as well as the illuminating beam has; neither slits extend to infinity nor illuminating waves in nature. Therefore, there will be a point after which a transition should be observed which would give rise to the emergence of the typical Fraunhofer diffraction structures. In such a case it is clear that within certain boundaries we will observe the Talbot pattern, but the latter will start to blur up out of them and will smoothly disappear to observe gradually the appearance of the Fraunhofer diffraction channels.[24] Instead of going to this limit by propagating further and further away quantum trajectories, let us rather consider the case where we increase the number of slits progressively until reaching a number such that within a certain bound region we have the certainty of observing a Talbot pattern, but that further away we will only see Fraunhofer diffraction channels. This transition can be observed, from top to bottom, in Fig. 4 with both ρ_t and the associated quantum trajectories.

As can be seen in Fig. 4(a), the lack of neighboring trajectories allows the trajectories to spread out in all directions with no bound and therefore no pattern can be observed. Free propagation of a Gaussian wave packet just means, according to this trajectory picture, that one can observe free motion (rectilinear and uniform) as in classical mechanics almost since the beginning of the propagation. At the beginning, nonetheless, we have to take into account the fast motion resulting from the acceleration occurred by the release of the initial wave packet. This effect of fast motion is even stronger in the case of slits with unit transmission.[13] In terms of the standard quantum mechanics, this means that ρ_t spreads linearly in time, but keeping constant its volume (here each snapshot constituting the frames has been normalized to unit in order to be able to appreciate the shape of ρ_t at long times). This constant volume only means that the number of trajectories conserves although they are far apart one another.

When we consider two slits, as in Fig. 4(b), things change dramatically. From standard quantum–mechanical viewpoint we observe a channeled structure due to the interference of the two outgoing Gaussian wave packets. This is the Fraunhofer diffraction pat-

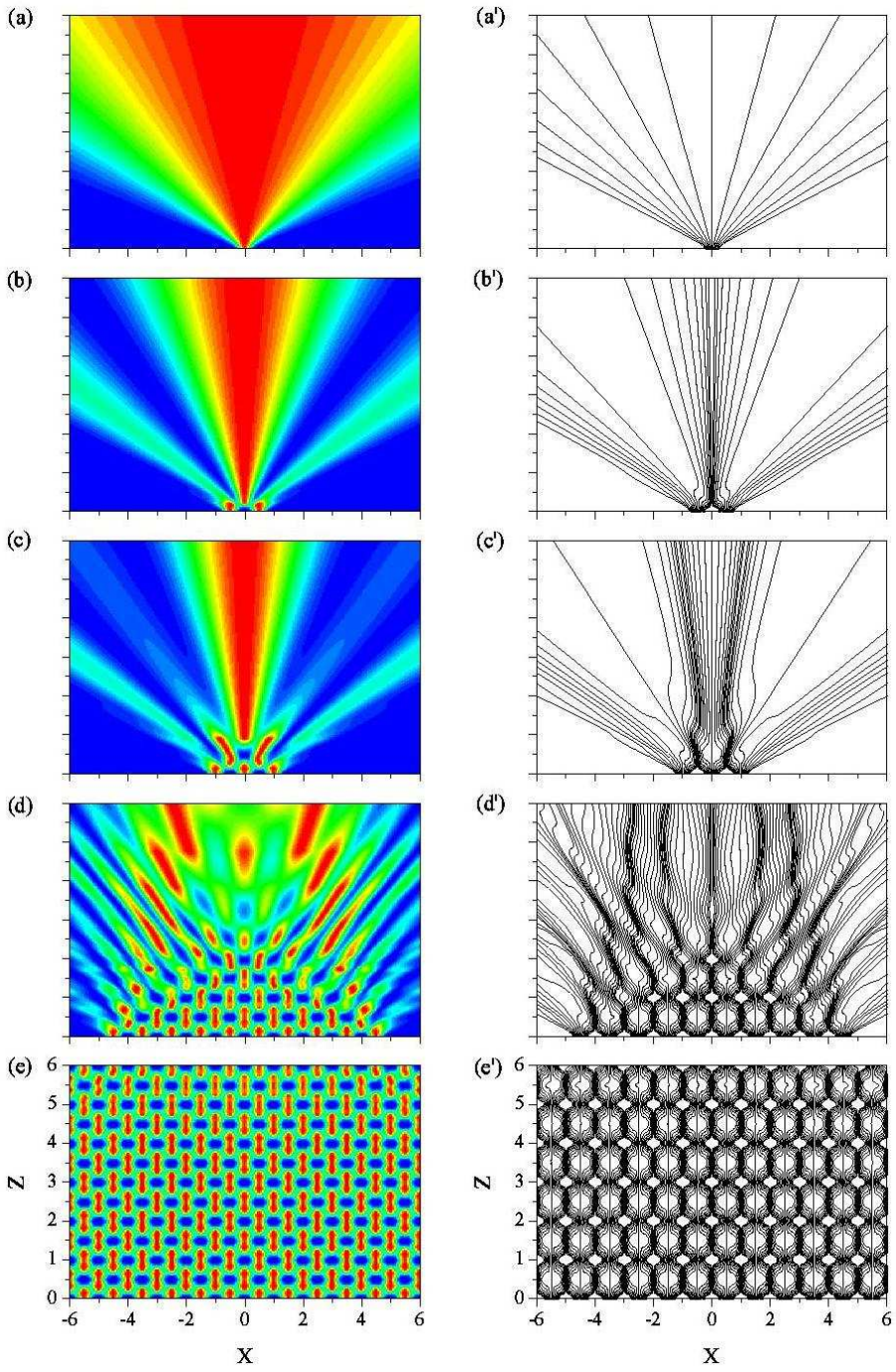

FIG. 4: (Color online.) Left: Appearance of the Talbot carpet within a certain space region as the number of slits increases: (a) $N = 1$, (b) $N = 2$, (c) $N = 3$, (d) $N = 10$, and (e) $N = 50$. Right: Quantum trajectories corresponding to the cases shown in the left panels. In all panels, the x–distance is scaled in units of the grating period (d), and z in units of twice the Talbot distance ($2z_T$).

tern. From the quantum trajectory viewpoint, though we also observe that the trajectories leave along those different channels (with a very low density of trajectories in between), it is remarkable the fact that the semi–plane behind the slits has been divided in two identical halves, where trajectories undergo a specular motion, but never crossing to the half dominated by the opposite slit. There is a very strong quantum pressure exerted by the trajectories arising from each half along the symmetry axis of the system. Moreover, it is also worth commenting that very close to the slits there is a brief resemblance of a certain pattern, with two temporary maxima just be-

hind the slits. This increases in Fig. 4(c), where we can observe three maxima, and then another two behind as a result of an effect similar to that described when discussing Fig. 3(b). After that, any possibility of a Talbot pattern disappears and the Fraunhofer diffraction channels emerge immediately. Note, nonetheless, that now the space is divided into three region, two specular, and a central one in between which increases linearly once the Fraunhofer limit is reached.

From the previous comments we can then establish that the Talbot effect can be seen as a "partition" of the space as the number of slits increases because of the strong effect (acting as an infinite barrier) of the quantum pressure. This is confirmed when we go to $N = 10$ [see Fig. 4(d)] and $N = 50$ [see Fig. 4(d)]. Indeed, the existence of the quantum pressure leads to a sort of quantum equilibrium state in which the unit structures formed by the bunches of trajectories can coexist. Only when the quantum pressure starts decreasing, these units begin to blur up since the trajectories spread out the corresponding boundaries. Since this effect is similar to a dissipation, it could be called a quantum trajectory dissipation. This nonequilibrium situation remains until a new equilibrium is established: the Fraunhofer regime.

As has been seen, the topology of the trajectories is very different in each of the regimes mentioned above, Talbot and Fraunhofer. This is because of the type of condition that gives rise to each one. In the Talbot equilibrium regime one has a constraint: quantum trajectories can only move along straight channels in front of their corresponding slits. This gives rise to a pattern that is stationary itself when looking at the momentum representation: each unit structure can be seen as the result of a spreading and compressing Gaussian function confined within a square box, which is characterized by a well defined momenta spectrum. When the constraint (the square box) breaks, there is a redistribution of momenta that ends up in the quantized momenta corresponding to the Fraunhofer channels. In this case, we have a single momentum for each channel, and the particles will display stationarity in a space representation, i.e., the profile of ρ_t will remain the same (regardless its relative maximum). The momenta that contribute to modulate the evolution along the Talbot pattern are precisely those that later on will separate to give rise to the different Fraunhofer channels!

Note that this comment is important when one wants to construct either Talbot or Fraunhofer patterns experimentally, or to study them from a theoretical viewpoint. Moreover, one must realize that the stationarity of the Talbot regime is only typical of this near field phenomenon. In general, near field or Fresnel phenomena are not stationary. Nonetheless, as we will see in next Section, one can still speak about a certain class of stationarity (in the momentum space) within the Fresnel diffraction regime different from that observed in a Talbot regime.

On the other hand, it is precisely the fact that the motion is constraint along channels within the Talbot regime what makes this problem to resemble that of a multimode cavity. In this case, the sum of modes (momentum spectrum in our case) gives rise to different types of evolution, but always repetitive and characterized by a certain frequency, that of the slower mode.[19]

V. ATOM–SURFACE SCATTERING

Talbot patterns are not only characteristic when having slit arrays. As said above, they appear whenever one deals with infinitely periodic structures in which interference can be observed. This happens, for example, when we have a typical atom–surface scattering system.[13,25] In Fig. 5 we can see the formation of the Talbot pattern when we have a beam of He atoms targeting ten unit cells of the Cu(110) surface at perpendicular incidence and energy $E_z = 21$ meV. This scattering system is described by a classical interaction potential $V(x, z) = V_M(z) + V_C(x, z)$, where

$$V_{\rm M}(z) = D(1 - e^{-\alpha z})^2 - D \tag{39}$$

is a Morse potential, and

$$V_{\rm C}(x, z) = De^{-2\alpha z}\left[0.03\ \cos\left(\frac{2\pi x}{d}\right) + 0.0004\ \cos\left(\frac{4\pi x}{d}\right)\right], \tag{40}$$

the coupling term between the two degrees of freedom. Here, $D = 6.35$ meV, $\alpha = 1.05$ Å^{-1}, and $d = 3.6$ Å (as the aperture of the slit).[24,26] The corrugation of the surface is very weak as can be appreciated by the amplitudes of the cosine functions.

In order to make the plot clear, we have neglected the incident part of the trajectories, and considered as before, the evolution of those corresponding to the centroid line of the incoming wave, parallel to the surface. As can be seen in Fig. 5(a), the pattern is very similar to that displayed by the $N = 10$–slit system plotted in Fig. 4(d). This is because the corrugation of the surface is relatively weak. This can also be seen if we compare Figs. 5(b) and 3(b); though the latter has been obtained considering $N = 50$, the structure is similar in both cases (we are inside the Talbot area). Note, however, that the Talbot structure repeats a bit further away than twice the Talbot distance considered before ($2d^2/\lambda$). The reason for this shift is because of the attractive part of the interaction potential, $V(x, z)$, which causes a certain acceleration in the motion of the particles. This is the so–called *Beeby correction* in atom–surface scattering.[10] In other words, only when the potential is flat, we can assume that $z_T = d^2/\lambda$. Otherwise, we should consider an effective Talbot distance,

$$\tilde{z}_T \equiv \frac{d^2}{\tilde{\lambda}(x, z)} = z_T\sqrt{1 - \frac{V(x, y)}{E_z}}, \tag{41}$$

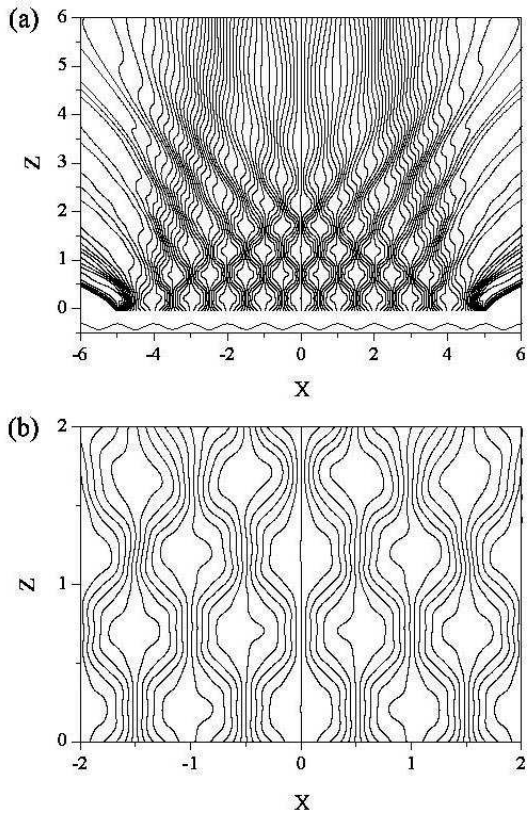

FIG. 5: (a) Quantum trajectories corresponding to the He–Cu(110) system at 21 meV and normal incidence. Only the emergent part has been plotted. (b) Enlargement of the trajectories shown in part (a). In both panels, the x–distance is scaled in units of the Cu(110) unit cell (d), and z in units of twice the Talbot distance for an N–slit grating ($2z_T = 2d^2/\lambda$).

where $\tilde{\lambda}(x,z) = 2\pi\hbar/\sqrt{2m[E_z - V(x,z)]}$. Taking into account that $V(x,z) < 0$, it is clear that the factor $V(x,y)/E_z$ in Eq. (41) will be greater than 1, and therefore $\tilde{z}_T > z_T$. The correction factor in Eq. (41) due to the presence of the well depth is $\sqrt{1 + D/E_z}$, and therefore we obtain $\tilde{z}_T/z_T = 1.14$, which is basically the discrepancy observed in Fig. 5(b). Hence, within the context of atom–surface scattering, it would be appropriate to speak about the *Talbot–Beeby effect*, which gathers both the effects caused by the periodicity (depending on V_C) and those arising from the attractive interaction (depending on V_M).

It is clear that since there is no an infinite beam of He atoms illuminating the Cu surface, the quantum pressure will decrease as the atoms get further from the surface and the Talbot pattern will disappear. However, there is something very interesting in this kind of systems: one can extract already very important information about the diffraction peaks (experimentally detected at Frauhofer distances) once the classical asymptotic region is reached ($V \simeq 0$). This is a nice manifestation of the effect mentioned above: the motion within the Fresnel region is governed by the momenta that will give rise later on to the different Franhofer diffraction channels. This has been easily proven by Sanz *et al.*[24] by computing the S–matrix elements in the classical asymptotic region and comparing them with the intensity calculated from quantum trajectories collected in the asymptotic region. A similar calculation for slit systems by the same authors can be seen in Ref. 12. The Fraunhofer regime is reached very far from the region where the interaction potential V is negligible and increases its distance as the number of unit cells illuminated by the initial atomic beam is increased. Thus, for example, for ten unit cells the Fraunhofer regime is reached around 1000 Å.

VI. CORRESPONDENCE PRINCIPLE AND TALBOT EFFECT

As heavier impinging particles are considered, i.e., when we approach the classical limit the behavior is drastically different. In such a case the effects of the corrugation are more noticeable. If instead of He atoms we consider a fictitious particle with a mass 500 times that of a He atom, it is clear that quantum effects should disappear or, at least, decrease. This is what one could think, mistakenly, when observing Fig. 6(a), where we have represented the diffraction of such particles by a grating consisting of ten slits. As can be seen, the trajectories are basically straight lines, what induces to think that no interference effects are present (neither Talbot nor Fraunhofer ones)), but particles move tracing a simple rectilinear, uniform motion. Obviously, this is misleading; both the x and z directions are given in terms of the old d and z_T. However, if we replot this figure taking into account that now z_T has increased by a factor $\sqrt{m/m_{\rm He}}$ (where m is the mass of the fictitious particle), we obtain again a Talbot pattern. And far away we would find the same Fraunhofer pattern as before. What has happened is that particles move now more slowly, and therefore the spreading of the corresponding bunches of trajectories will also be slower.

The previous result shows that quantum particles remain quantum even in the so–called classical limit;[27] one only needs to be patient and wait time enough in order to observe again the quantum phenomena (of course, unless the complexity of the system is so enormous that any quantum effect is imperceptible experimentally). However, what happens if instead of ten slits we illuminate ten cells of the Cu(110) surface with a beam of our fictitious particle? The answer appears in Fig. 6(b): now the topology displayed by the quantum trajectories tries to resemble that of the classical one, but avoiding to cross. That is, since classical trajectories give rise to the appearance of two caustics (direction of maximal reflected intensity) at the so–called rainbow angles, the quantum trajectories will describe a similar structure, with the particularity that they cannot cross, and therefore, after tracing an almost straight line, they will be bounced backwards in relatively sharp angle, as seen in the lowest

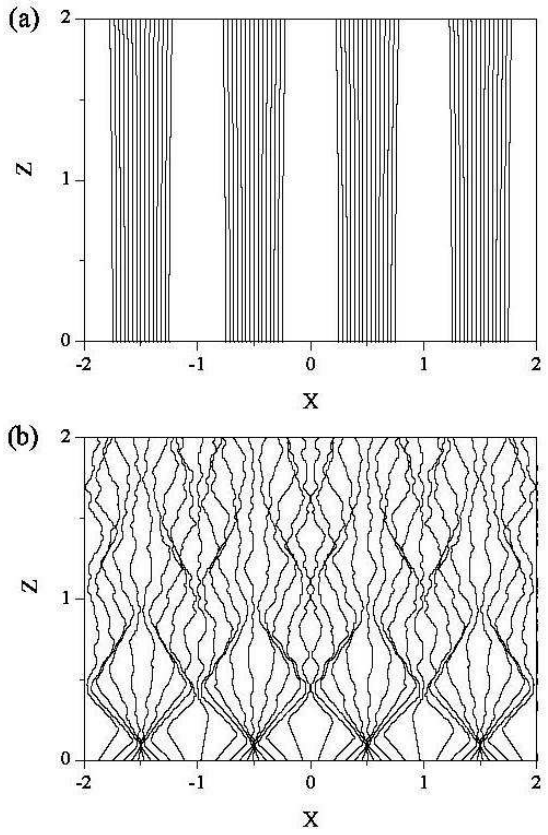

FIG. 6: Diffraction of a particle with a mass 500 times heavier than that of a He atom by: (a) 10 slits, and (b) 10 unit cells of the Cu(110) surface. In both panels, the x–distance is scaled in units of the Cu(110) unit cell (d), and z in units of twice the Talbot distance for an N–slit grating ($2z_T = 2d^2/\lambda$). Moreover, the perpendicular incidence energy is $E_z = 21$ meV in both cases.

part of Fig. 6(b). Of course, since this motion is very sharp and the number of slits is relatively restricted, the quantum pressure will decrease very fast and the corresponding unit structures will also disappear in a relatively fast manner. Moreover, notice that, because of this motion, the laminarity of the flow described by the trajectories is lost, and now their topology is more irregular and also showing that some of them cross (though such crossings are at different times).

VII. CONCLUSIONS

To conclude, there are three important points in this work that are worth stressing. First, the Talbot–Beeby effect is proposed to understand Talbot patterns in presence of attractive interaction potentials. Second, regardless the gradual spreading of the partial wave function associated to each unit cell of a periodic grating, the corresponding initial swarms of trajectories keep moving in a bound space region. To some extent, this is analogous to consider the trajectories moving inside a multimode cavity.[13,19] Because of this effect, within the Talbot interferometry context, the superposition principle in Bohmian mechanics has to be understood in a very different way as it is in standard quantum mechanics. It is not simply the overlapping of a number of wave functions, but allocation of identical copies of the same trajectory behavioral pattern. Third, in connection with this, this behavior is analogous to the classical behavior observed when studying periodic structures: all the information about the periodic structure can be obtained by simply studying the classical effects provoked by one of the periods.[12]

Acknowledgements

This work has been supported by the Spanish Ministry of Education and Science under the project with reference number FIS2004–02461. A.S. Sanz would also like to thank the Spanish Ministry of Education and Science for a "Juan de la Cierva" Contract.

* Electronic address: asanz@imaff.cfmac.csic.es
† Electronic address: s.miret@imaff.cfmac.csic.es

[1] H.F. Talbot, Philos. Mag. **9**, 401 (1836).
[2] L. Rayleigh, Philos. Mag. **11**, 196 (1881).
[3] M.S. Chapman, C.R. Ekstrom, T.D. Hammond, J. Schmiedmayer, B.E. Tannian, S. Wehinger, and D.E. Pritchard, Phys. Rev. A **51**, R14 (1995).
[4] L. Deng, E.W. Hagley, J. Denschlag, J.E. Simsarian, M. Edwards, C.W. Clark, K. Helmerson, S.L. Rolston, and W.D. Phillips, Phys. Rev. Lett. **83**, 5407 (1999).
[5] M. Berry, I. Marzoli, and W. Schleich, Physics World, **14**(6), 7 (2001).
[6] D. Wójcik, I. Bialynicki–Birula, and K. Zyczkowski, Phys. Rev. Lett. **85**, 5022 (2000).
[7] M. Berry, J. Phys. A: Math. Gen. **29**, 6617 (1996).
[8] M.J.W. Hall, M.S. Reineker, and W.P. Schleich, J. Phys. A: Math. Gen. **32**, 8275 (1999).
[9] E.J. Amanatidis, D.E. Katsanos, and S.N. Evangelou, Phys. Rev. B **69**, 195107 (2004).
[10] J.L. Beeby, J. Phys. **C4**, L359 (1971).
[11] J.T. Winthrop and C.R. Worthington, J. Opt. Soc. Am. **55**, 373 (1965).
[12] A.S. Sanz, F. Borondo, and S. Miret–Artés, J. Phys.: Condens. Matter **14** 6109 (2002).
[13] R. Guantes, A.S. Sanz, J. Margalef–Roig, and S. Miret–Artés, Surf. Sci. Rep. **53**, 199 (2004)
[14] N.W. Ashcroft and N.D. Mermin, *Solid State Physics* (Saunders College, Philadelphia, 1976).
[15] M. Born and E. Wolf, *Principles of Optics* (Pergamon Press, New York, 1980).

[16] A.E. Kaplan, P. Stifter, K.A.H. van Leeuwen, W.E. Lamb, Jr., and W.P. Schleich, Phys. Scrip. **T76**, 93 (1998).
[17] A.E. Kaplan, I. Marzoli, W.E. Lamb, Jr., and W.P. Schleich, Phys. Rev. A **61**, 032101 (2000).
[18] M. Nest, Phys. Rev. A **73**, 023613 (2006).
[19] A.S. Sanz, J. Phys. A: Math. Gen. **38**, 6037 (2005).
[20] D. Bohm, Phys. Rev. **85**, 166, 180 (1952).
[21] P.R. Holland, *The Quantum Theory of Motion* (Cambridge University Press, Cambridge, 1993).
[22] R.E. Wyatt, *Quantum Dynamics with Trajectories: Introduction to Quantum Hydrodynamics* (Springer, Berlin, 2005).
[23] In Bohmian mechanics a wave function is uniquely associated to one single particle. However, in agreement to the statistical postulate of the standard quantum mechanics, this particle can have any initial position x_0 with probability $\rho(x_0, 0)$. The results predicted by the standard quantum mechanics are reproduced by sampling all possible initial positions. This is equivalent to consider a system constituted by many *non–interacting* particles associated to the same wavefunction, and distributed according to $\rho(x, 0)$.
[24] A.S. Sanz, F. Borondo, and S. Miret–Artés, Phys. Rev. B **61**, 7743 (2000).
[25] A.S. Sanz and S. Miret–Artés, Phys. Rep. (in press).
[26] D. Gorse, B. Salanon, F. Fabre, A. Kara, J. Perreau, G. Armand, and J. Lapujoulade, Surf. Sci. **147**, 611 (1984); S. Miret–Artés, J. P. Toennies, and G. Witte, Phys. Rev. B **54**, 5881 (1996).
[27] A.S. Sanz, F. Borondo, and S. Miret–Artés, Europhys. Lett. **55** 303 (2001).